High-Bandwidth Embedded Rogowski Coil on Multilayer Substrate with Minimal Contribution to Power Loop Inductance

Takahiro Okamoto
Graduate School of Natural Science and Technology
Okayama University
Okayama, Japan
pnc26471@s.okayama-u.ac.jp

Masataka Ishihara
Graduate School of Natural Science and Technology
Okayama University
Okayama, Japan
masataka.ishihara@ec.okayama-u.ac.jp

Kazuhiro Umetani
Graduate School of NaturalScience and Technology
Okayama University
Okayama, Japan
umetani@okayama-u.ac.jp

Eiji Hiraki
Graduate School of NaturalScience and Technology
Okayama University
Okayama, Japan
hiraki@okayama-u.ac.jp

***Abstract*— Power devices using GaN-HEMTs require high-bandwidth current sensors for fast switching current sensing, switch device protection and system control. PCB-embedded Rogowski coils are suitable for high frequency current sensing because they are electrically non-contact, have no magnetic core, and can be compactly mounted in the system. However, in conventional Rogowski coils, it is necessary to pass the current path through the center of the coil. This causes an extension of the current path, and consequently, an increase in parasitic inductance in the power loop of GaN-HEMT devices. In this paper, we propose a Rogowski coil consisting of a multilayer printed-circuit-board (PCB) substrate, which pick-up coil embedded in a laminated bus bar. The pick-up coil is also designed with microstrip lines to allow measurement of high-frequency current. Experimental results confirm that the bus bar of the proposed Rogowski coil exhibited low parasitic inductance and can detect high-frequency currents.**

Keywords—Current sensor, Parasitic Inductance, Laminated bus bar, Microstrip line, Impedance matching

I. INTRODUCTION

The next-generation semiconductor GaN-HEMT, which has emerged in recent years, achieves low on-resistance and high-speed switching. Consequently, inverters using GaN-HEMT can miniaturize surrounding passive components through increased drive frequency, which has led to extensive research and development of compact, high power density inverters and converters to date [1]–[3]. In such power modules employing GaN-HEMT, a current sensor in the switching current measurement module is required for device protection and system control. Additionally, since the short-circuit withstand capability of GaN-HEMTs is limited [4], a high-bandwidth current sensor capable of instantaneously detecting abnormal currents is essential.

As shown in Fig. 1, the Rogowski coil consists of a coil winding and an integration circuit. The basic current measurement principle of the Rogowski coil is that the

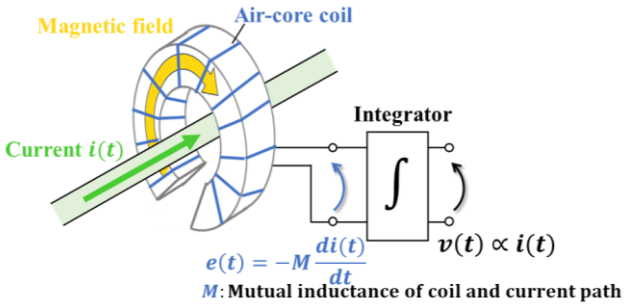

Fig. 1. Structure of Rogowski Coil

alternating magnetic field generated by the current links with the coil, inducing a voltage across the coil windings proportional to the derivative of the current according to Faraday's law of electromagnetic induction. This induced voltage is then integrated by the integrator, allowing the current to be detected. The Rogowski coil is electrically non-contact with the current and does not use a magnetic core, making it widely used as a current sensor for power devices, In recent years, compact Rogowski coils designed on PCB substrates have been actively researched and developed [5]–[8].

However, the conventional Rogowski coil structure shown in Fig. 1 presents two challenges. The first is the low bandwidth of the coil winding. To accurately detect fast-rising currents, such as those generated by GaN-HEMTs, it is difficult to achieve accurate measurement with existing Rogowski coils, which have a bandwidth of around 100 MHz. The second challenge is the increase in parasitic inductance associated with the implementation of the Rogowski coil. In conventional Rogowski coil structures, the current path must pass through the center of the coil, requiring the current path to be routed out and reconnected when implementing the Rogowski coil in a power module. This increases the length of the current path and, consequently, the parasitic inductance along the path. An increase in parasitic inductance in the power loop of power devices can cause significant switching surges in semiconductor

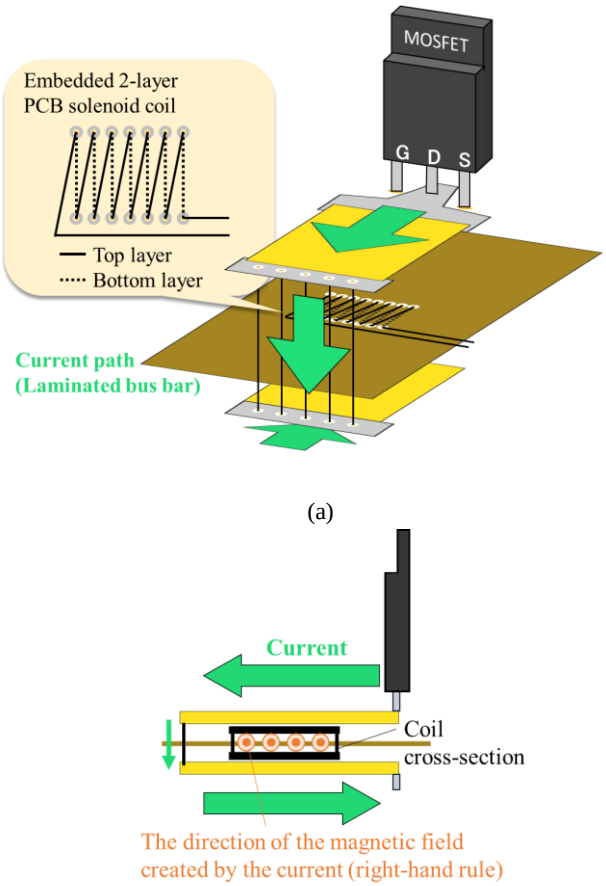

Fig. 2. Coil structure of Embedded Rogowski Coil (a), (b) side view

devices, posing a risk of device and system failure. Additionally, the need to route the current path through the coil center limits the width of the current path to the coil diameter, making it difficult to secure sufficient current path width for handling large currents.

To address the first issue of low bandwidth in the coil winding, the study in [9] designs the Rogowski coil winding as a microstrip transmission line with characteristic impedance, with both ends terminated by resistors for impedance matching. This approach suppresses the high-frequency reflection of voltage and current, characteristic of high-frequency regions, thereby preventing the degradation of the coil winding's frequency response. To address the second issue of increased parasitic inductance, an embedded Rogowski coil structure, as shown in Fig. 2, has been proposed [10]–[12]. As shown in Fig. 2(a), the current flows in opposing directions in a laminated structure, with the coil winding embedded inside as a solenoid coil formed within a two-layer substrate. According to Fig. 2(b), the magnetic field generated by the opposing currents links with the embedded coil winding in the same direction, inducing a voltage across the coil winding proportional to the derivative of the current, enabling current detection based on the same principle as conventional Rogowski coils. Meanwhile, the magnetic fields generated externally by the opposing currents cancel each other out, thereby minimizing the increase in parasitic inductance caused by the implementation of the Rogowski coil [13].

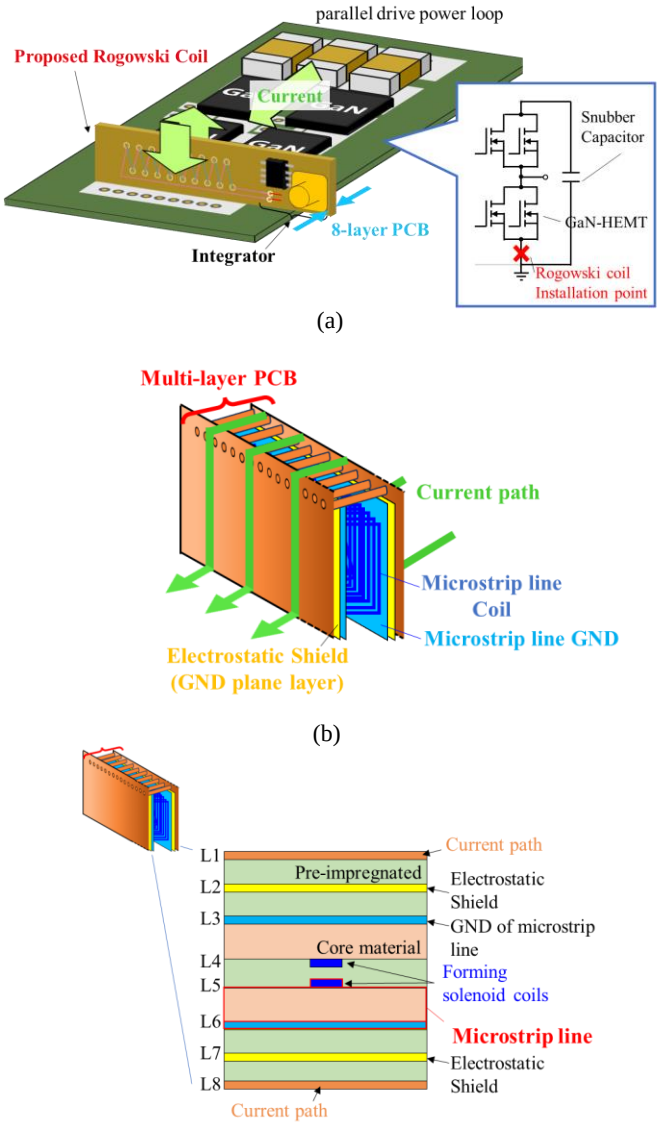

Fig. 3. Schematic diagram of the proposed embedded Rogowski Coil. (a) Example of implementation in a GaN-HEMT power module. (b) Schematic diagram. (c) 8-layer substrate configuration.

In this study, a high-bandwidth embedded Rogowski coil, constructed using a multi-layer PCB, is proposed to simultaneously address both challenges. The proposed Rogowski coil minimizes the increase in parasitic inductance, and through impedance matching, enhances the bandwidth of the coil winding. The effectiveness of the proposed Rogowski coil is verified by evaluating both the suppression of parasitic inductance and the improved high-bandwidth performance of the coil winding.

II. The Proposed Coil Structure of Rogowski Coil

Fig. 3 shows a schematic of the proposed embedded Rogowski coil. The proposed Rogowski coil consists of an 8-layer PCB, and, as shown in Fig. 3(a), it is mounted vertically relative to the horizontal power loop current path of the GaN-HEMT parallel-driven power module. Since the surface layer of the proposed structure serves as a laminated current path, it

minimizes the increase in parasitic inductance caused by the installation of the Rogowski coil. As shown in Fig. 3(c), the coil winding is formed as a solenoid-type coil using the signal lines of the microstrip line on layers 4 and 5. The ground (GND) of the microstrip line utilizes the adjacent layers, 3 and 6, respectively. Thus, the coil winding functions as a transmission line with characteristic impedance, enabling impedance matching at both ends of the coil winding. This suppresses voltage and current reflections during high-frequency current measurement and increases the bandwidth of the coil winding. To prevent noise caused by electrostatic coupling of high-frequency currents flowing on the surface layer and interference from external electromagnetic noise, electrostatic shielding layers connected to GND are implemented on layers 2 and 7 of the microstrip line's GND layer. Since the electrostatic shielding layers must be connected to GND, the Rogowski coil needs to be installed at the low-side GaN-HEMT source terminal (GND).

III. Layout of the Proposed Rogowski Coil

A. *The current path*

As shown in Fig. 5(a) and Fig. 5(e), the current path is arranged on the 1st and 8th layers. The current path on the 1st layer is connected to 50 Ω from the signal line of the SMA edge connector. It forms an opposing trace that connects to the GND of the SMA edge connector on the lower side of the layout on the 8th layer through a via on the upper side of the layout. The 50 Ω resistor ensures impedance matching with the characteristic impedance of the measurement equipment when measuring the transfer characteristics of the Rogowski coil. The path width of the current route is designed to correspond to the switching current path width of a parallel-driven GaN-HEMT power module.

B. *Microstrip line coil*

The coil winding is formed as a solenoid coil using the inner 4th and 5th layers, as shown in Fig. 5(d). The 4th and 5th layers are connected via buried via holes. The coil winding has an inter-winding spacing at least 10 times the width of each line, and the 3rd and 6th layers are used as the ground for the microstrip line, enabling the design as a microstrip line with characteristic impedance, as shown in Equation (1) [13]. The GND layers of the 3rd and 6th microstrip lines are connected by vias in the central part of Fig. 5(c). This approach eliminates paths for eddy currents to flow via the vias with respect to the magnetic flux linked to the coil winding, thus stabilizing the microstrip line's GND. Where ε_r is the relative permittivity of the dielectric, w is the line width, t is the copper thickness, and h is the layer spacing, designed to achieve a characteristic impedance of 47 Ω.

$$Z_0 = \frac{87}{\sqrt{\varepsilon_r + 1.41}} \ln\left(\frac{5.98h}{0.8w + t}\right) \quad (1)$$

Additionally, the self-inductance of the coil winding is approximately 75nH, as calculated using equation (2), where μ_0 is the permeability of free space and l_{track} is the length of the coil winding.

$$L_s = \frac{\mu_0 l_{track}}{2\pi} \ln\left(\frac{5.98h}{0.8w + t}\right) \quad (2)$$

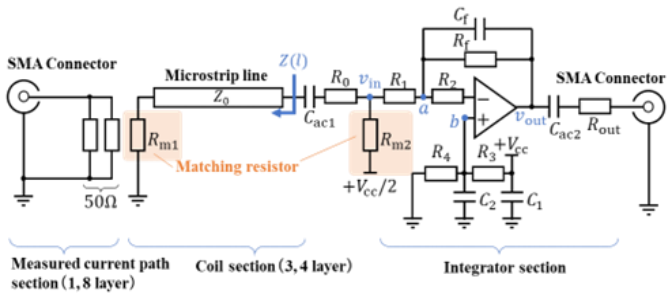

Fig. 4. Proposed structure characteristic evaluation circuit

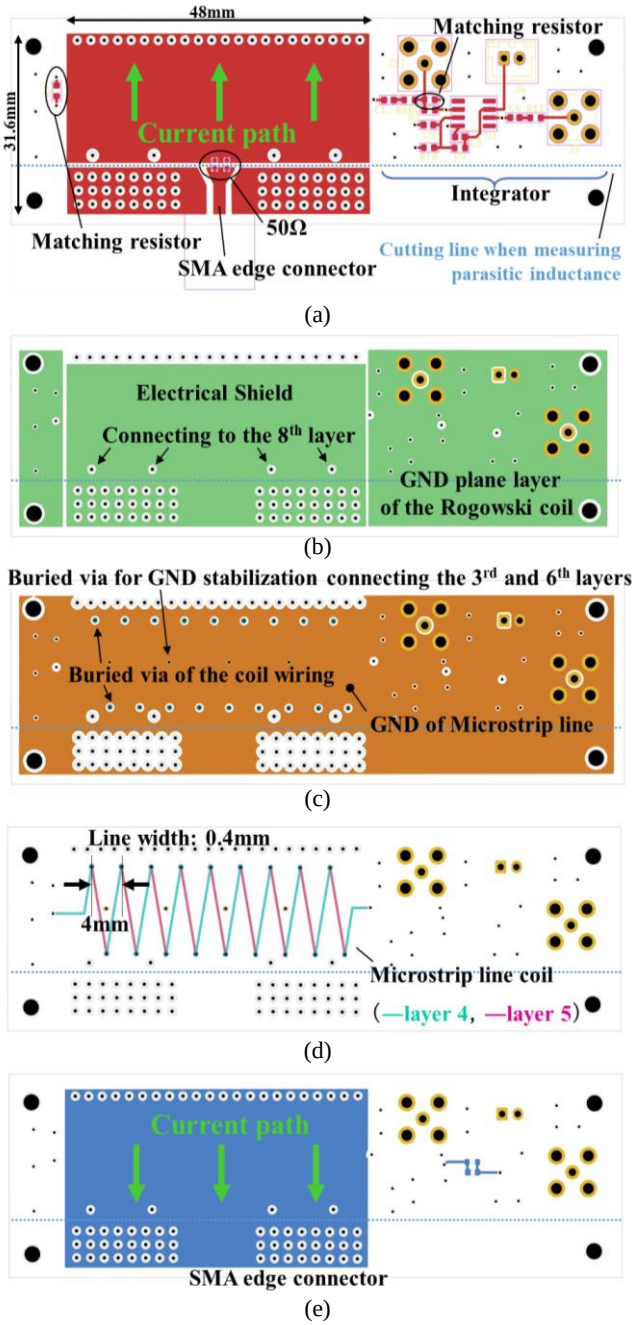

Fig. 5. PCB layout of the proposed Rogowski coil. (a)layer 1 (b) layer 2, 7 (c) layer 3, 6 (d) layer 4, 5 (e) layer 8

C. Electrical Shield

A GND plane electrostatic shield is provided on layers 2 and 7, where the coil winding is embedded. This shield prevents interference from noise caused by electrostatic coupling of high-frequency currents on the surface layer and external electromagnetic noise from affecting the GND of the microstrip line on layers 3 and 6. Since the electrostatic shield must be connected to GND, the proposed Rogowski coil must be attached to the source terminal of the low-side GaN-HEMT in the inverter. To establish the opposing current path, the electrostatic shield is connected to the 8th layer via a through-hole on the lower side of the layout in Fig. 5(b).

D. Integrator

The integrator, as shown in Fig. 4, is designed as an inverting integrator using an operational amplifier (THS3201 from Instruments). The transfer function is shown in equation (3), and the cutoff frequency of the integrator is shown in equation (4). The integrator's low-frequency gain is set to $R_f/R_1 = 10$, with a cutoff frequency of $f_c = 700$[kHz]. The component values for the integrator are listed in Table 1. The circuit layout utilizes layers 1 and 8, with all inner layers designated as GND planes.

$$G(\mathrm{j}\omega) = -\frac{R_f}{R_1}\frac{1}{1+\mathrm{j}\omega C_f R_f} \tag{3}$$

$$f_c = \frac{1}{2\pi C_f R_f} \tag{4}$$

The capacitors C_{ac1} and C_{ac2} act as coupling capacitors, blocking DC current, and can be considered shorted in the AC equivalent circuit. The resistor R_2 is used to prevent oscillations in the current-feedback operational amplifier and is connected to the inverting input terminal of the op-amp. The resistor R_{out} sets the output impedance of the integrator, matching it to the impedance of the subsequent stage. Meanwhile, the input impedance of the integrator can be expressed by Equation (5). Due to the virtual short of the op-amp, points a and b maintain equal potential, effectively making points an equivalent to GND in the AC equivalent circuit. Thus, the input impedance of the integrator can be represented as the combined impedance of R_1 and R_{m2}, ensuring impedance matches with the characteristic impedance of the coil winding in the previous stage.

$$Z_{in} = \frac{R_1 \cdot R_{m2}}{R_1 + R_{m2}} \tag{5}$$

IV. Evaluation

A. Evaluation of Parasitic Inductance in the Current Path

The surface layout of the measurement board for assessing the parasitic inductance of the measured current path is shown in Fig. 6. The backside of the measurement board is a ground plane, where current flows directly beneath the surface current and is connected to the SMB connector's ground pin through via holes. By comparing the parasitic inductance in the current path with the Rogowski coil attached at the mounting position shown in Fig. 6 and without the coil (connected with copper foil instead), the parasitic inductance of the Rogowski coil itself is determined. This parasitic inductance is calculated by connecting a capacitor in parallel with the current path parasitic inductance at the base of the SMB connector and deriving it from the parallel resonance point of the impedance characteristic.

TABLE I. PARAMETERS OF THE INTEGRATORS

Symbols	Values
R_1	$110[\Omega]$
R_2	$510[\Omega]$
R_3,R_4	$10[k\Omega]$
R_f	$560[\Omega]$
R_{out}	$51[\Omega]$
C_1	$0.1[\mu F]$
C_2	$4.7[\mu F]$
C_f	$390[pF]$
C_{ac1},C_{ac2}	$4.7[\mu F]$

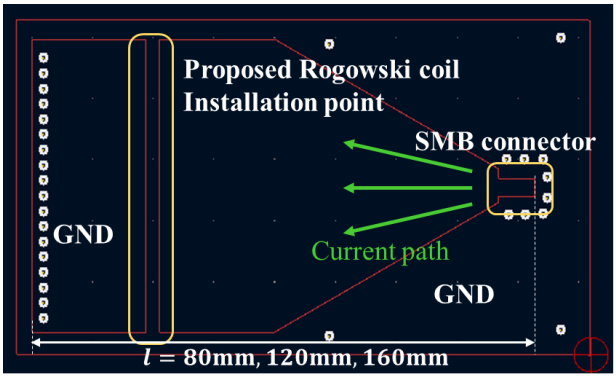

Fig. 6. Top layout for parasitic inductance measurement

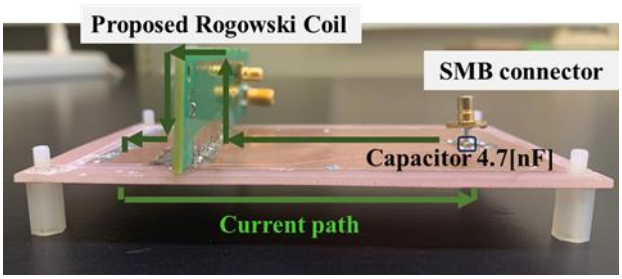

Fig. 7. Side view of parasitic inductance measurement board

Since the capacitor includes parasitic elements, the precise parasitic inductance is extracted by fitting the parallel resonance characteristics obtained in circuit simulation—considering the equivalent circuit model with parasitic components of the capacitor—to the measured resonance characteristics.

A side view of the measurement board with the Rogowski coil attached is shown in Fig. 7. An impedance analyzer (IM7581, HIOKI) was used for impedance measurement, and a 4.7 nF capacitor (KEMET) was employed. The equivalent circuit model accounting for parasitic components of the capacitor was obtained from the KEMET website. The current path length was varied to 80[mm], 120[mm], and 160[mm], and impedance characteristics for each were measured. Fig. 8 shows the relationship between the current path length and the parasitic inductance with and without the Rogowski coil attached. From Fig. 8, the differential parasitic inductance of the current path indicates that the parasitic inductance of the proposed Rogowski coil is consistently very low, remaining below 1[nH].

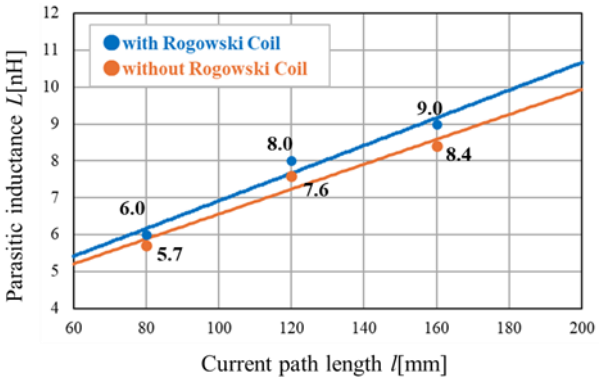

Fig. 8. Parasitic inductance characteristics

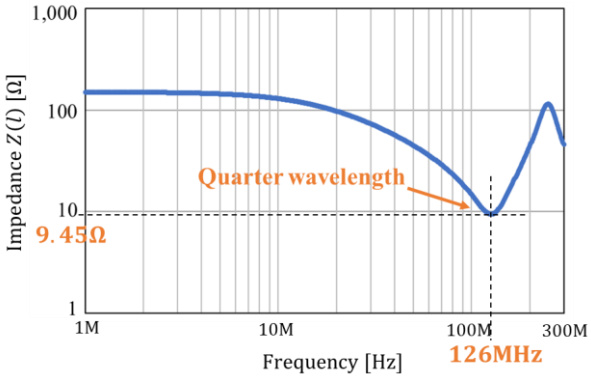

Fig. 9. Input impedance characteristics

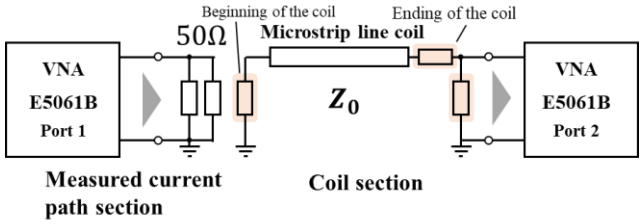

Fig. 10. Circuit for measuring coil transfer characteristics

B. *Transfer Characterisitc of the Proposed Rogowski Coil*

First, the characteristic impedance of the designed microstrip line is derived. Equation (6) shows the relationship between the characteristic impedance and the coil input impedance $z(\lambda/4)$ when the wavelength is one-fourth. Based on Equation (6), the characteristic impedance of the microstrip line can be determined by connecting an arbitrary resistor R_{m1} at the start of the coil and measuring the coil's input impedance at one-fourth wavelength.

$$Z(\lambda/4) = Z_0 \frac{R_{m1} + \mathrm{j}Z_0 \tan(\pi/2)}{Z_0 + \mathrm{j}R_{m1} \tan(\pi/2)} = \frac{{Z_0}^2}{R_{m1}} \qquad (6)$$

Fig. 9 shows the frequency characteristics of the coil input impedance when 150 Ω is connected to the starting end of the coil. The impedance was measured using an impedance analyzer (HIOKI, IM7581). According to Equation (6), at the frequency where the wavelength is one-fourth, the input impedance consists only of a real component, displaying resonance characteristics. Therefore, the impedance at one-fourth wavelength corresponds to the peak value in the frequency response. Based on Equation (6), the characteristic impedance was found to be 37.6[Ω]. Compared to the design value of 47 [Ω], the derived value is smaller, likely due to the prepreg thickness between layers 3-4 and 5-6 of the microstrip line being thinner than the nominal value.

Next, we measure the impedance matching and transmission characteristics of the proposed Rogowski coil structure at the coil's start and end points, both in matched and mismatched conditions. Fig. 10 shows the circuit diagram for measuring the transmission characteristics, using a vector network analyzer (Keysight, E5061B). In the case of impedance matching at the coil's start, a 36 Ω resistor is connected, and in the mismatched case, a 0 Ω resistor is used. At the coil's end, a 130 Ω resistor is connected in parallel when matching the impedance, ensuring that the combined impedance with the network analyzer's 50 Ω coaxial cable matches the characteristic impedance of the coil windings. In the mismatched case, a 1 kΩ resistor is added in series. Fig. 11 shows the transmission characteristics of the coil winding in both matched and mismatched conditions. Fig. 11 shows that the gain increases with a slope of +20[dB/dec] from 1MHz to about 100MHz during impedance matching and mismatching, respectively, and that a voltage proportional to the derivative of the current under test is induced between the coil windings. The phase characteristic shows -90 degrees at a few MHz but begins to change significantly at tens of MHz This is because, at these frequencies, the wavelength of the measured current becomes non-negligible compared to the coil winding length, causing the voltage induced in the coil to not remain constant along the coil, resulting in phase shifts. Fig. 11(a) shows that impedance matching at the beginning of the coil gives transfer characteristics that suppress the quarter-wavelength resonance characteristics. Additionally, matching the impedance at the coil's end increases the gain of the output characteristic. This is because matching the coil's end ensures that the induced voltage is transmitted without reflection between the coil and the integrator, maximizing the power transfer.

The transmission characteristics of the proposed Rogowski coil, from the measured current path to the output of the integrator circuit, are shown in Figure 12. In this configuration, both the start and end points of the coil (including the input impedance of the integrator circuit) are matched to the characteristic impedance of the coil. The circuit constants for the integrator are shown in Table 1. Fig. 12 shows that the gain characteristics of the Rogowski coil are flat and constant up to 100MHz. This flat characteristic is equivalent to the combined gain of the coil and the integrator circuit, indicating that the Rogowski coil outputs a voltage that is a scaled version of the measured current. However, beyond 100 MHz, the frequency response exhibits characteristics that combine the resonance of the coil and the oscillatory behavior that may arise from the integrator circuit. In this frequency range, the measured current cannot be detected accurately. Regarding the phase characteristic of the Rogowski coil, it is found that, like the gain, the phase is a combination of the phase characteristics of the coil and the integrator circuit. This means that the phase between the measured current and the voltage output from the Rogowski coil is not constant. This variation in phase is likely due to the propagation of the induced voltage along the microstrip coil, and compensatory circuitry for phase shift needs to be considered.

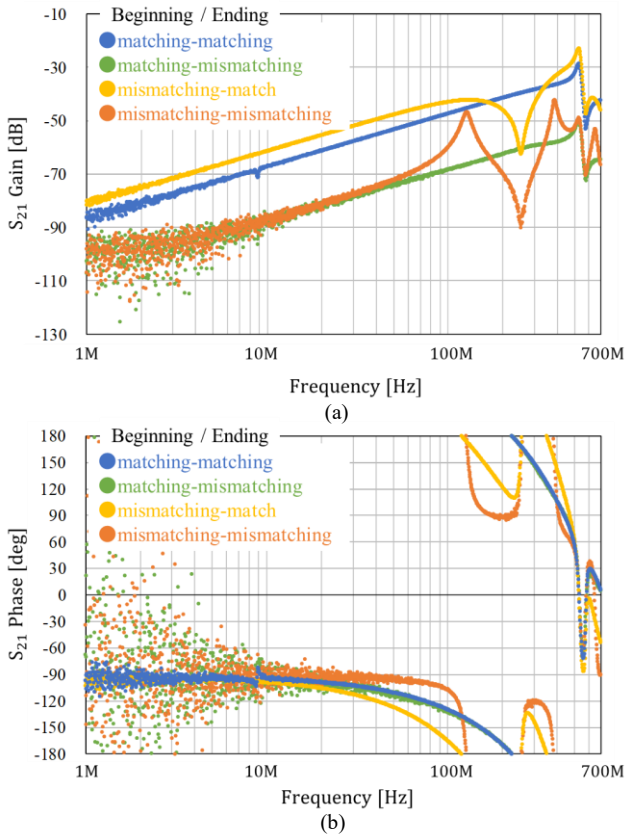

Fig. 11. Coil transfer characteristic. (a) Gain characteristic. (b) Phase characteristics

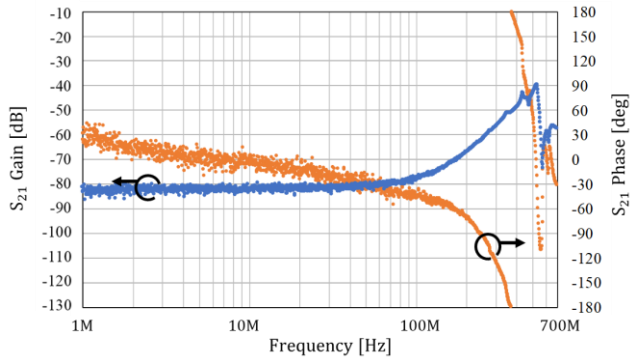

Fig. 12. Transfer characteristic of the proposed Rogowski coil

Furthermore, the bandwidth of the proposed Rogowski coil structure is limited by the integrator circuit, which restricts its effective range to around 100MHz. Improving the bandwidth of the integrator circuit will be an important future challenge.

V. Conclusion

In this study, a new embedded Rogowski coil with an electrostatic shield composed of multilayer substrates is proposed as a current sensor for GaN-HEMT power modules, which does not contribute to an increase in parasitic inductance. From the parasitic inductance evaluation, it was confirmed that the parasitic inductance of the current path under test is small, less than 1[nH], and that the increase in parasitic inductance caused by the extension of the current path can be minimized. Experiments also confirmed the effectiveness of the impedance matching in the proposed Rogowski coil and the ability to accurately detect the current under test, based on the gain characteristics of the frequency response measurement of the coil. However, the bandwidth limitation of the integrating circuit remained an issue. Therefore, improving the bandwidth of the integrating circuit is a future issue.

References

[1] N. G. M. Thao, K. Naruse and K. Fujisaki, "Reduction of Harmonics and Inverter Temperature in Experimental GaN-based Motor Drive System at High Frequencies Using LC Filter," 2022 IEEE Ninth International Conference on Communications and Electronics (ICCE), Nha Trang, Vietnam, 2022, pp. 507-512

[2] D. Nehmer, M. Hepp, W. Wondrak and M. -M. Bakran, "Switching a eMode GaN HEMT under conditions of an inverter module for electrical vehicles (EV)," 2023 25th European Conference on Power Electronics and Applications (EPE'23 ECCE Europe), Aalborg, Denmark, 2023I. S. Jacobs and C. P. Bean, “Fine particles, thin films and exchange anisotropy,” in Magnetism, vol. III, G. T. Rado and H. Suhl, Eds. New York: Academic, 1963, pp. 271–350.

[3] P. Han, P. Liu, Q. Huang, Z. Chen and A. Q. Huang, "A 650 V, 2.1 mohm GaN Half-bridge Power Module for 400V EV Traction Inverter Application," 2022 IEEE Energy Conversion Congress and Exposition (ECCE), Detroit, MI, USA, 2022, pp. 1-6

[4] D. Bisi et al., "Short-Circuit Capability with GaN HEMTs : Invited," 2022 IEEE International Reliability Physics Symposium (IRPS), Dallas, TX, USA, 2022, pp. 1-7

[5] P T Nandh Kishore, Sumit Kumar Pramanick, and Soumya Shubhra Nag, “Development of a PCB Embedded High Bandwidth Coil Based Current Sensor Suitable for Characterizing GaN Devices”, 2023 11th International Conference on Power Electronics and ECCE Asia (ICPE 2023 - ECCE Asia), Jeju Island, Korea, 2023, pp99-104

[6] H. Li, Z. Xin, X. Li, J. Chen, P. C. Loh and F. Blaabjerg, "Extended Wide-Bandwidth Rogowski Current Sensor With PCB Coil and Electronic Characteristic Shaper," in IEEE Transactions on Power Electronics, vol. 36, no. 1, pp. 29-33, Jan. 2021

[7] Y. Shi, Z. Xin, P. C. Loh and F. Blaabjerg, "A Review of Traditional Helical to Recent Miniaturized Printed Circuit Board Rogowski Coils for Power-Electronic Applications," in IEEE Transactions on Power Electronics, vol. 35, no. 11, pp. 12207-12222, Nov. 2020

[8] T. Tao, Z. Zhao, W. Ma, Q. Pan and A. Hu, "Design of PCB Rogowski Coil and Analysis of Anti-interference Property," in IEEE Transactions on Electromagnetic Compatibility, vol. 58, no. 2, pp. 344-355, April 2016

[9] Y. Wang *et al.*, "Transmission Line Rogowski Coil: Isolated Current Sensor With Bandwidth Exceeding 3 GHz for Wide-Bandgap Device," in IEEE Transactions on Power Electronics, vol. 38, no. 11, pp. 13599-13605, Nov. 2023

[10] L. Zhao, J. D. van Wyk and W. G. Odendaal, "Planar embedded pick-up coil sensor for power electronic modules," Nineteenth Annual IEEE Applied Power Electronics Conference and Exposition, 2004. APEC '04., Anaheim, CA, USA, 2004, pp. 945-951 vol.2

[11] Y. Xue, J. Lu, Z. Wang, L. M. Tolbert, B. J. Blalock and F. Wang, "A compact planar Rogowski coil current sensor for active current balancing of parallel-connected Silicon Carbide MOSFETs," 2014 IEEE Energy Conversion Congress and Exposition (ECCE), Pittsburgh, PA, USA, 2014, pp. 4685-4690

[12] Y. Kuwabara, K. Wada, J. -M. Guichon, J. -L. Schanen and J. Roudet, "Implementation and Performance of a Current Sensor for a Laminated Bus Bar," in IEEE Transactions on Industry Applications, vol. 54, no. 3, pp. 2579-2587, May-June 2018

[13] A. Sagehashi, K. Kusaka, K. Orikawa, J. -i. Itoh and A. Momma, "Pattern design criteria of main circuit using printed circuit boards for parasitic inductance reduction," 2014 16th International Power Electronics and Motion Control Conference and Exposition, Antalya, pp. 569-574, Turkey, 2014